Computers & Geosciences 89 (2016) 144–160

Contents lists available at ScienceDirect

Computers & Geosciences

journal homepage: www.elsevier.com/locate/cageo

Case study

Spatial analysis for susceptibility of second-time karst sinkholes: A case study of Jili Village in Guangxi, China

Guoqing Zhou [a,*], Hongbo Yan [a,b], Kunhua Chen [a], Rongting Zhang [a]

[a] Guangxi Key Laboratory of Spatial Information and Geomatics, Guilin University of Technology, Guilin 541004, China
[b] College of Geomatics and Geoinformation, Guilin University of Technology, Guilin 541004, China

ARTICLE INFO

Article history:
Received 27 September 2015
Received in revised form
31 January 2016
Accepted 1 February 2016
Available online 2 February 2016

Keywords:
Subsidence hazard
Susceptible map
Logistic regression model
GIS database
Impact factor

ABSTRACT

After a big karst sinkhole happened in Jili Village of Guangxi, China, the local government was eager to quantitatively analyze and map susceptible areas of the potential second-time karst sinkholes in order to make timely decisions whether the residents living in the first-time sinkhole areas should move. For this reason, karst sinkholes susceptibility geospatial analysis is investigated using multivariate spatial data, logistic regression model (LRM) and Geographical Information System (GIS). Ten major karst sinkholes related factors, including (1) formation lithology, (2) soil structure, (3) profile curvature, (4) groundwater depth, (5) fluctuation of groundwater level, (6) percolation rate of soil, (7) degree of karst development, (8) distance from fault, (9) distance from the traffic route, and (10) overburden thickness were selected, and then each of factors was classified and quantitated with the three or four levels. The LRM was applied to evaluate which factor makes significant contributions to sinkhole. The results demonstrated that formation lithology, soil structure, profile curvature, groundwater depth, ground water level, percolation rate of soil, and degree of karst development, the distance from fault, and overburden thickness are positive, while one factor, the distance from traffic routes is negative, which is deleted from LRM model. The susceptibility of the potential sinkholes in the study area is estimated and mapped using the solved impact factors. The susceptible degrees of the study area are classified into five levels, very high, high, moderate, low, and ignore susceptibility. It has been found that that both very high and high susceptibility areas are along Datou Hill and the foothills of the study area. This finding is verified by field observations. With the investigations conducted in this paper, it can be concluded that the susceptibility maps produced in this paper are reliable and accurate, and useful as a reference for local governments to make decisions regarding whether or not residents living within sinkhole areas should move.

1. Introduction

Karst sinkholes is one of six major geological disasters, which include earthquake, collapse, landslide, debris flow, ground fissures and ground subsidence. It has widely been recognized that 16 countries will be and/or are encountering severe karst sinkhole disasters (Chen and Jin, 1992; Youssef et al., 2012; Frumkin, 2013, Kranjc, 2013; Van Westen, 2013; Gutiérrez et al., 2015; Carbonel et al., 2015). China is one example because the carbonate area covers as much as 3,440,000 km^2, accounting for 1/3 of China's land area (Shi and Liang, 1997). It has been reported that a total of 2087 karst sinkholes occurred in 2013 in China, and the City of Laibin is notorious for having the most severe karst sinkhole areas in China. It is estimated that 216 karst sinkholes have occurred in Laibin (Liu, 2013). One severe karst sinkholes occurred in the Jili Village of the City of Laibin on June 3, 2010, which caused six deaths, destroyed more than 100 houses, damaged numerous power transmission equipment and numerous farmlands, and caused severe mountain and ground cracks. It is estimated that the direct economic loss reached US $1,632,493 (http://news.sina.com.cn/c/2010-06-05/080420416918.shtml).

In order to minimize second-time karst sinkhole destruction effect, the local government was requested to determine the degree of susceptibility and subsequently make decisions concerning whether the residents should emigrate from severe susceptible areas. For this reason, this paper investigates and classifies the degrees of susceptibility of areas after first time karst sinkholes in Jili Village of the City of Laibin, Guangxi, China. Related methods for identifying susceptible areas have been previously reported. These methods and their advantages and disadvantages can be categorized and analyzed as follows:

(1) *Qualitative approaches*: Qualitative methods are usually based on inventory maps and depend on expert opinions to rank the

* Corresponding author.
E-mail address: gzhou@glut.edu.cn (G. Zhou).

http://dx.doi.org/10.1016/j.cageo.2016.02.001
0098-3004/

importance of the factors influencing sinkholes (Raghu, 1984; Aronn, 1991; Mejia-Nabarro and Luis, 1996; Li and Zhou, 2003; Deborah and Waleed, 2002; Gao et al., 2005; Gutiérrez-Santolalla et al., 2005; Farrant and Cooper, 2008; Mancini et al., 2009). These methods are ultimately validated through field analysis. The major advantage of qualitative methods is that they consider a number of site impact factors, which are combined to make judgments. The disadvantage is that there is a level of arbitrariness in making these judgments, and the precision and accuracy of recognizing susceptible areas is theoretically difficult to assess. For example, the method of fuzzy comprehensive evaluation has been employed by several researchers to produce implicit rules for recognizing the degrees of susceptibility of different areas. Although this method has reached full automation at each processing step, it is difficult to obtain the state score factors and the factor weights (Kaufmann and Quinif, 2002; Işık, 2007; Choi et al., 2010; Waele et al., 2011).

(2) *Quantitative approaches*: Quantitative methods originate from mathematical statistical approaches that are carried out by determining the correlation between impact factors and sinkholes (Yilmaz, 2007; Galve et al., 2008, 2009a,b, 2015; Lee et al., 2010; Hyun and Saro, 2010; Gómez-Ortiz and Martín-Crespo, 2012; Taheri et al., 2015). Many methods, such as the analogy monitoring method (Kim, 2006), probabilistic theory (Galve et al., 2009a,b), traditional statistical analysis (Lee et al., 2010), value of information method (Kim, 2006), and artificial neural network (Kim et al., 2009), have been proposed in past decades. In particular, linear and nonlinear regression methods have widely been applied to estimate and evaluate geological disasters, such as those reported by Lee and Min (2001), Ayalew and Yamagishi (2005), Lulseged and Hiromitsu (2005), Lee and Sambath (2006), Bathrellos et al. (2009), Tao et al. (2010), and Wang et al. (2012). Each of these quantitative methods has its shortcomings. For example, the results produced by the fuzzy uncertainty method are difficult for experts to interpret and verify because the model is too ideal; various uncertain factors are not considered simultaneously (Kyriaki et al., 2013). However, the logistic regression model (LRM) overcomes this shortcoming because it can effectively determine the relationship between a dichotomous response and variables, whereas traditional multivariate linear regression methods cannot. In particular, the LRM method can simultaneously handle both continuous and discrete variables, which are not needed in normal distributions. The LRM method can also effectively recognize areas susceptible to other geological disasters such as landslides (Lamelas et al., 2008; Verachtert et al., 2011).

This paper attempts to assess the degree of susceptibility of a first-time karst sinkhole region. The study area in Jili Village, Guangxi, China is chosen to assess our method.

2. Study area and data set

2.1. Study area

Jili Village, located in the middle of Guangxi, China, covers approximately 5 km^2 and is centered at 109°10′50″E and 23°35′34″N. The landscape contains corrosion accumulation and a residual peak simple plain. An isolated karst peak is located in the center of the area. Sparse vegetation is located at the top of the peak, and bare bedrocks are observed everywhere. Karst sinkholes occurred in the hill valley and the foothill region on June 3, 2010 (see Fig. 1).

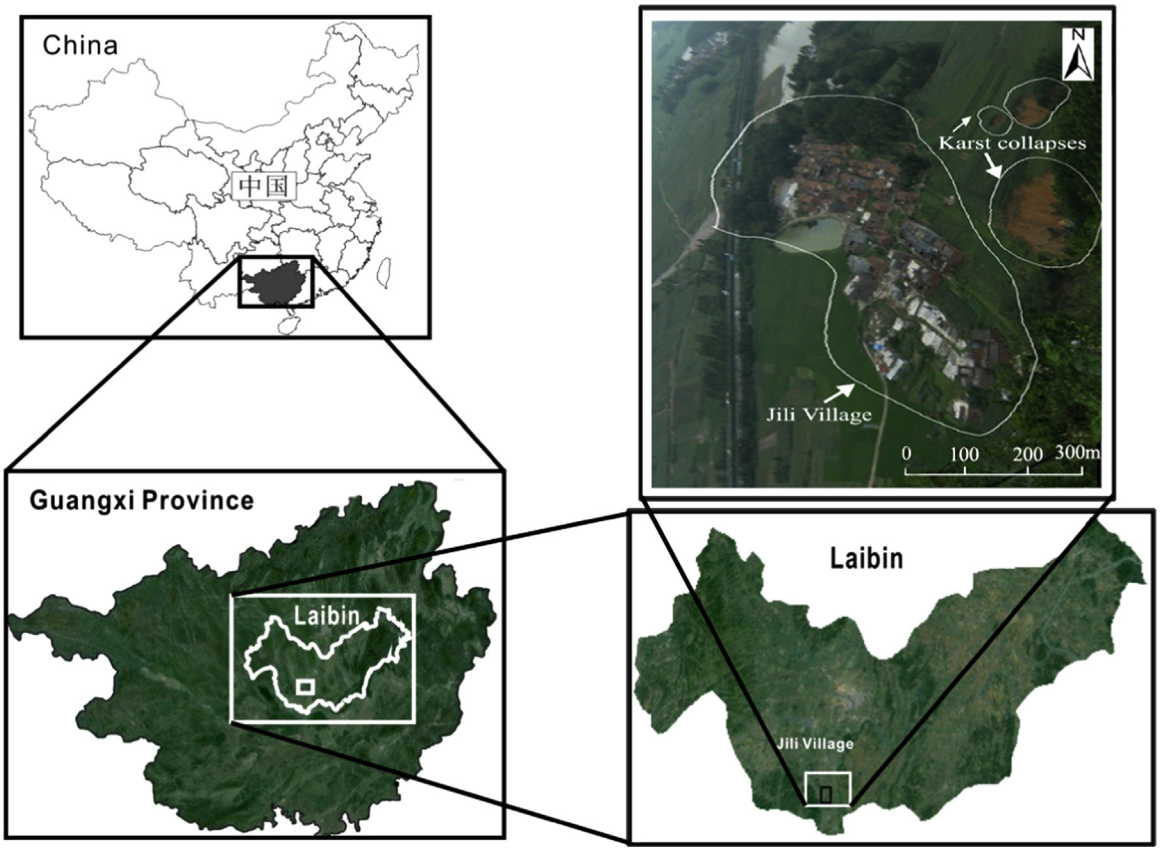

Fig. 1. Study area.

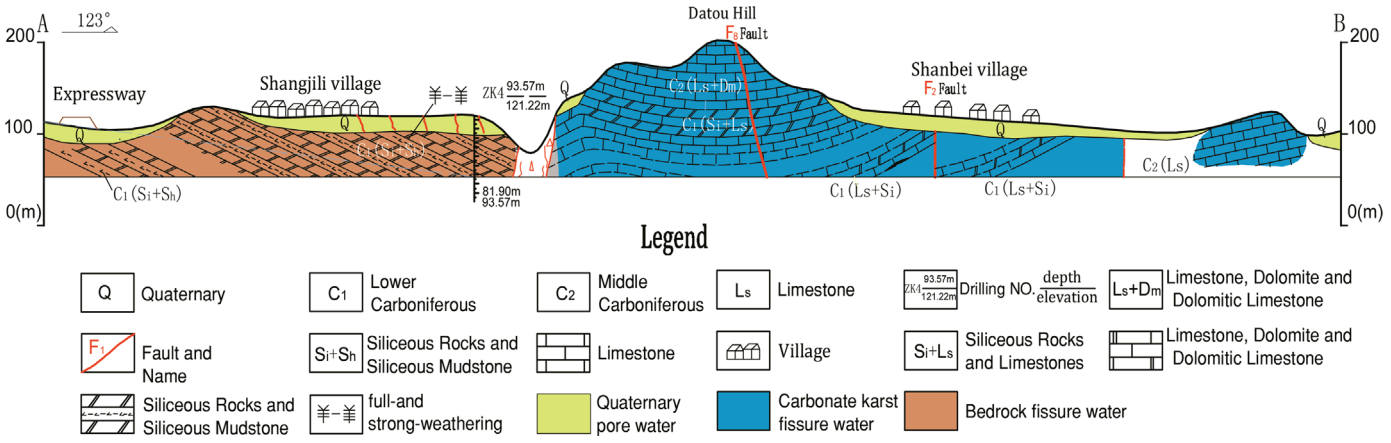

Fig. 2. Lithology cross-section of the study area (Courtesy of Hydrological geology engineering team of Laibin, 2010).

The study area is a typical subtropical monsoon climate, with warm temperatures and long hours of sunshine year-round. The interannual variation of precipitation in the area is large from April to September during the rainy season, and rainfall days account for more than 3/4 of the year. The groundwater is rich with spring flow at a rate of 100–1336.5 L/s. A river named *Hongshui River*, which is located 25 km north of Jili Village, is the groundwater drainage of the study area. The annual average flow of Hongshui River is nearly 2000 m^3/s; the maximum average flow is about 15,000 m^3/s; the minimum average flow is about 286 m^3/s; and the annual runoff is approximately 608.3×10^8 m^3 (Laibin hydrological monitoring station).

Strata of the study area tend to the east, and the strata lithology is complex and changeable. Influenced by the South and North tectonic system and the new China tectonic system, the rock strata are squeezed, dragged, flexed and fractured, so rock mass integrity is very poor. Field investigation found that the dip angle of the rocks is generally less than 15°. The lithology from the old to the new exposure is: Lower Carboniferous (C_1), Middle Carboniferous (C_2), Lower Cretaceous (K_1) and Quaternary (Q) (Fig. 2), and the location of the cross section AB is shown in Fig. 3.

Karst sinkholes are located on the axis of secondary fold of east wing syncline of Pingtang and west wing syncline of Laibin. In the middle there is a hill named Datou hill, whose syncline has been broken. The east wing syncline is Quaternary, drilling verification for siliceous rock and limestone. Attitude of bed in the axial part of the syncline is gentle, with west side 85–95°∠15–20°, east side 325–330°∠20°.

The geologic structure of the study area is very complex. Karst sinkholes have occurred in the shield part of Epsilon-type structure, which likes a Chinese sonogram, with a tectonic line lying nearly in the north-south direction. A normal fault, named *small Pingyang*, lies 3 km west from the sinkhole area. Folds and fractures are formed on the mountains. This area is recognized as the HuangLong limestone group of the carboniferous system. The limestone has been weathered. There are many large fully developed karst conduits in the mountain area. There are nine faults in the study area, five of which (denoted F1, F2, F7, F8, and F9 in Fig. 3) lie along the North-North-East distributions parallel to the fold axial; and four of which (denoted F3, F4, F5, and F6 in Fig. 3) lie along the North-West-West distributions parallel to the large fault (Li, 1984; Zhong et al., 1984; Zhou et al., 2014). In conjunction with their shifts, these faults form what is known as a *checkerboard pattern* (Fig. 3).

After referencing the basic geological data and hydrological data, combined with field investigation, it is preliminary judged that the potential occurrence are caused by:

(1) The depths of overburden thickness are quite thin and the rocks are easily to be dissolved.
(2) It is an area with quite complex geologic structure, and the karst sinkholes were located on the fault zone, with fractured rock mass.
(3) There are large karst pipelines in the hills, karsts were well-developed and the groundwater circulation is strong.
(4) The torrential rain after drought is the direct reason for karst sinkholes.

2.2. Data sets

The data sets used in this study contain the following:

(1) *Geographical data*: The geographical data includes a terrain contour map with a scale of 1:5000 created in July 2010, a mining well distribution map with a scale of 1:5000 created in July 2010, aerial photos acquired in June 2013, and relevant documents for geologic data from the Geological Environment Monitoring Station of the City of Laibin, Guangxi, China.
(2) *Geological data*: The geological data includes a geological map with a scale of 1:5000 created in July 2010, a quaternary soil structure map with a scale of 1:5000 created in July 2010, and geodetic positions of the sinkholes were measured by hand-GPS in July 2010. The size and shape of the sinkholes are measured by a laser range finder. The formation lithology data were obtained by drilling in July 2010, and the overburden thickness of the soil was measured by geological radar via high-density resistivity measurements (detailed parameters are shown in Table 1). Other data sets contain soil permeability and soil sampling data.
(3) *Digital elevation model (DEM)*: The digital elevation model was obtained by digitizing a 1:5000 hardcopy map; and saving the map as a DEM with a grid size of 10 m × 10 m using ArcMap software.
(4) *Hydrological data*: The hydrological data includes a hydrology map with a scale of 1: 100,000, and a groundwater contour map with scale of 1:5000 edited in July 2010.

The details of the collected data are listed in Table 2.

3. Data processing

3.1. Data pre-processing

Data pre-processing involved a data quality check, data format conversion, spatial coordinate transformation, projection transformation, coordinate registration and map vectorization. The pre-processing flowchart is depicted in Fig. 4.

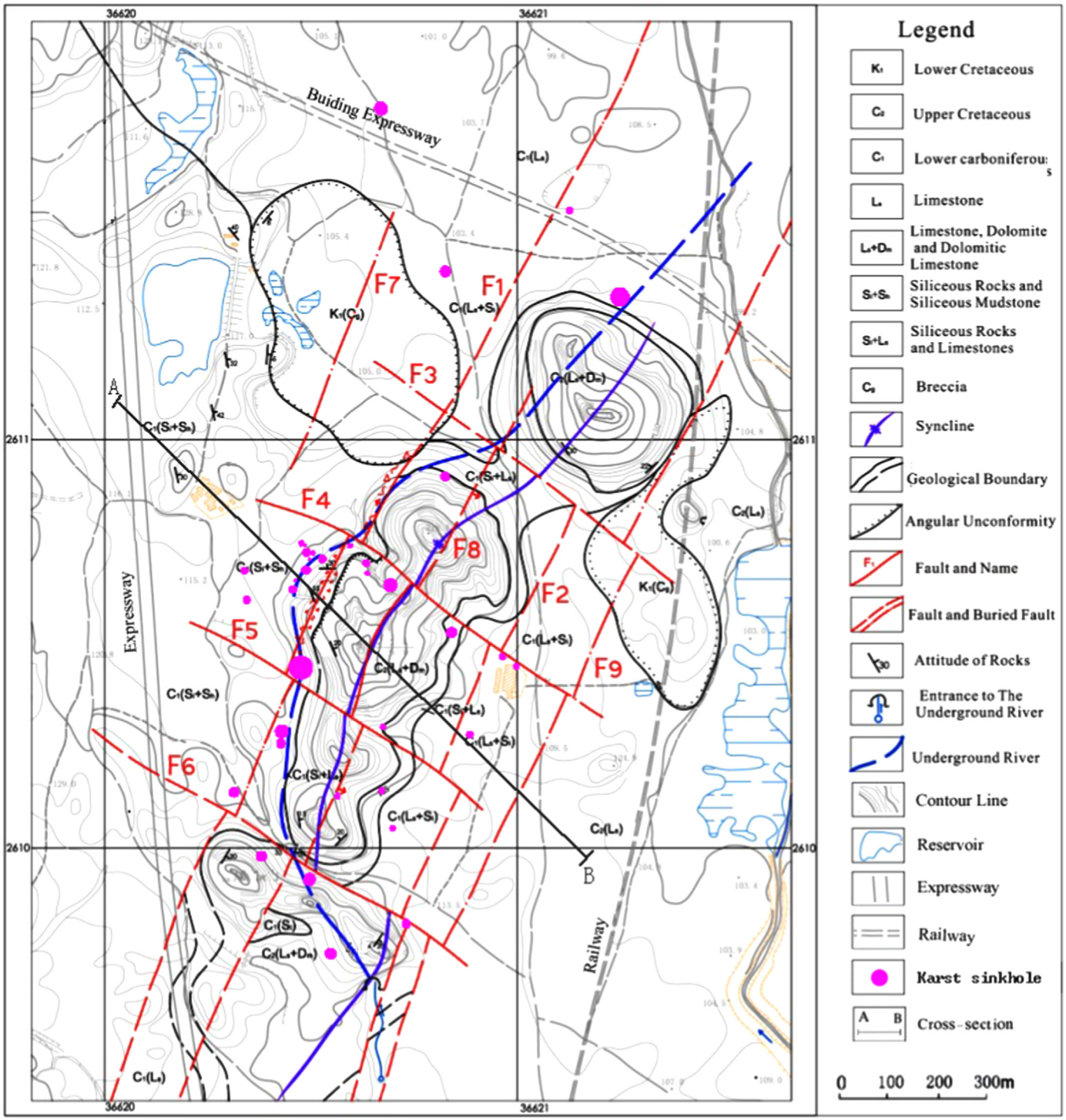

Fig. 3. Faults distribution in the study area (Courtesy of Laibin hydrological monitoring station, 2010).

Table 1
Detailed parameters of the geological radar used.

Radar type	Antenna	Sampling frequency	Number of sampling points	Sampling interval	Superposition times
MALA ProEx	50 MHz	512 MHz	500	0.3 m	128

To the further processing, the data in the database are normalized to a same scale and Gauss–Kruger projection coordinate system, which is a three-degree zone in the Xi'an 80 coordinate system, China.

3.2. Data management

The data for karst sinkholes analysis are derived from multi-source spatial data sets, typically graphic data and attributes data. The graphic data can be divided into vector data and raster data.

Table 2
Details of the collected data.

File name	File Type	Coordinate system	Scale	Coordinate Transform	Production year
Hydrology geological	Paper map	Xi'an 1980	1: 100,000	No	1997
Groundwater level	Paper map	Xi'an 1980	1:5000	No	2010
The structure of soil	Paper map	Xi'an 1980	1:5000	No	2010
Sinkholes distribution	CAD	Beijing 1954	1:5000	Yes	2010
Formation lithology	CAD	Beijing 1954	1:5000	Yes	2010
geological map of bed rocks	CAD	Beijing 1954	1:5000	Yes	2010

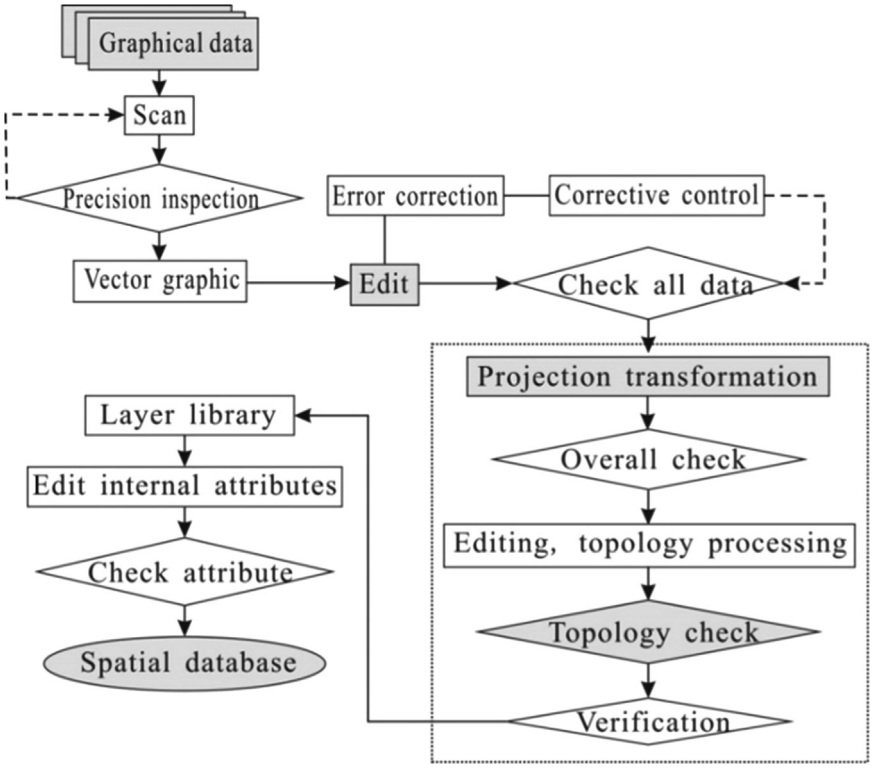

Fig. 4. Flowchart of data pre-processing.

Vector data include data pertaining to geological lithology, fault structure, and land use. Raster data include DEMs. The attribute data are stored in a data table that includes disaster attributes and environmental attributes. Disaster attributes include farmland destruction, damaged roads, destroyed houses and other economic loss data. Environmental attributes include land use attributes, geological lithological attributes and landform attributes. ArcGIS version 9.3 was employed to effectively manage the multi-source data collected (Chen, 2008). The technological process is depicted in Fig. 5.

3.2.1. Spatial data management

Three layers for the three categories of spatial data, geographical data, geological data, and hydrological data, were created using ArcGIS. Each of the layers contains different types of spatial data. For example, the geographical layer consists of such elements as transportation, land use and land cover, residences, and wells. The geological layer consists of such elements as soil structure, soil hole, soil thickness and characteristics, crack, fault, karst, karst sinkholes, and geological radar layout. The hydrological layer consists of the following elements: groundwater depth, groundwater runoff, groundwater undulation, groundwater characteristics, and reservoir.

3.2.2. Attribute data management

Factors including type, length, and precision of attribute data were formulated for the different types of spatial data. The attribute data were input by connecting the map to the attributes files using ArcGIS software. As shown in Table 3, the data type, length, decimal for groundwater depth (m) were text, 50, and 2, respectively. An example for description of a karst sinkhole, which includes ID, name, sinkhole date, *XY* coordinates, shape, slope, depth, length, and level.

4. Spatial analysis

4.1. Selection of impact factors

Many factors affect karst sinkholes. These factors mainly include karst development, groundwater, overburden, topography and human activities. The conditions relevant to karst development include the degree of karst development and rock mass structure; groundwater conditions include groundwater depth, fluctuation frequency, fluctuation level and runoff intensity; overburden conditions include overburden thickness and soil structure; and human activities mainly include artificial pumping intensity. Based on early published literature (Galve, et al., 2008, 2009a,b, 2015; Kyriaki et al., 2013), the results obtained from the field investigation and available data, 10

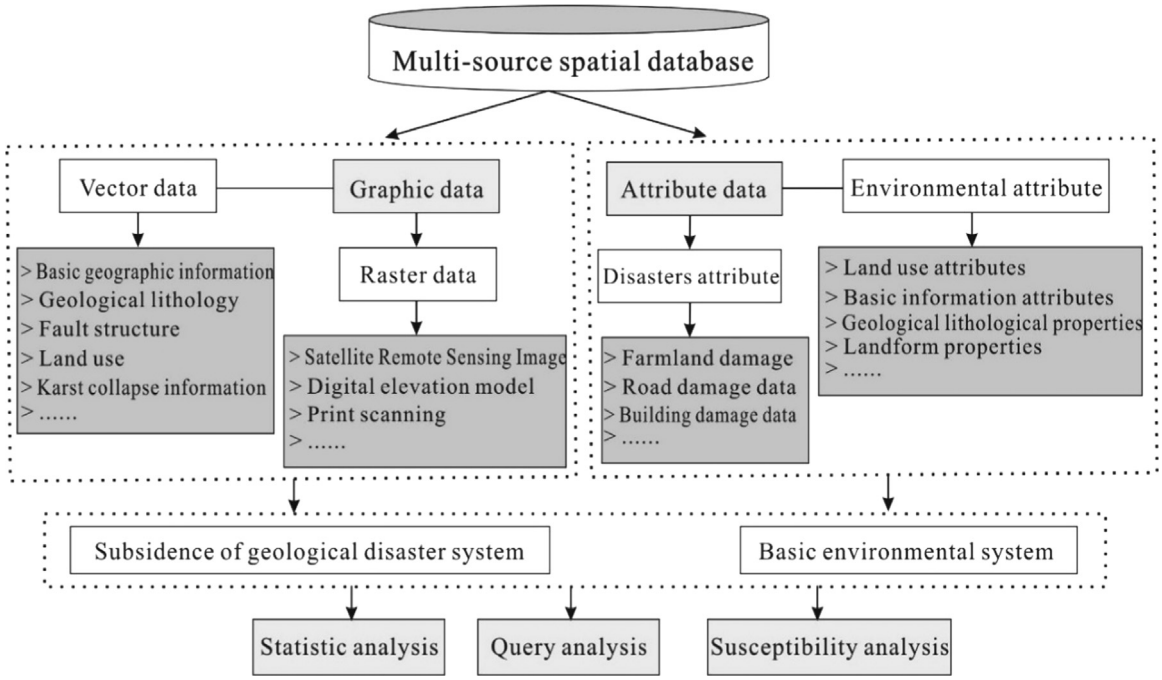

Fig. 5. Spatial database management framework of the collected sinkholes data.

Table 3
Attribute table of data structure.

Field name	Data type	Length	Decimal
Name of sinkholes	Text	50	
Name of traffic route	Text	50	
Area (m^2)	Numerical value	8	1
Groundwater depth (m)	Numerical value	16	2
Percolation rate of soil	Numerical value	8	2
Soil structure	Float	16	
Formation lithology	Character	30	
.....	.....	.....	

factors are initially selected in this paper: (1) formation lithology, (2) soil structure, (3) profile curvature, (4) groundwater depth, (5) fluctuation of groundwater level, (6) percolation rate of soil, (7) degree of karst development, (8) distance from fault, (9) distance from the traffic route, and (10) overburden thickness.

4.2. Quantity of impact factors

The LRM model only handles the numerical values of these impact factors, the first task is therefore to quantify the factors selected above. The grid size of each factor must be unified before the factors are quantified. The layer data are raster using ArcMap software based on the multi-source spatial database established in Section 3. According to Li and Zhou (2003), a 10 m pixel resolution from 1:5000 scaled hardcopy map was selected. The principle is as follows:

$$G_s = 7.49 + 0.0006S - 2.0 \times 10^{-9}S^2 + 2.9 \times 10^{-15}S^3 \quad (1)$$

Where G_s represents the size of the grid, S represents scale denominator of the base map, which is 5000 in this study. a 10 m pixel resolution is calculated according to formula (1). There are a total of 48,100 pixels which contain 185 columns and 260 rows. In this paper, the quantification method is proposed as follows:

1) Take the selected factors as the first level, and then classify the first level factors into the sub-levels;
2) Retrieve the grid number at a resolution of 10 m × 10 m (corresponding DEM grid size) from the sub-level layer;
3) Calculate the ratio of the factor of the classified sub-level layers using the relation

$$x_{ij} = \frac{N_{ij}}{S_{ij}} \quad (2)$$

where $i=1, 2, \ldots, n$, represents the sequence number of the first factor level; $j=1, 2, \ldots, m$ represents the sequence number of the second factor level; N_{ij} represents the number of grid sinkhole disaster points within the region of the secondary factor; S_{ij} represents the area of the secondary factor; x_{ij} is the value required for the secondary factor. The index value computed by Eq. (2) is an indication of how much the factor contributes to the karst sinkholes.

With the proposed impact factor quantity method, the details of each of impact factor are quantified as follows.

4.2.1. Formation lithology

Formation lithology is one of the most important causes of karst sinkholes (Yuan, 2013). Geophysical field exploration (e.g., drilling), and other comprehensive investigations have revealed that factors such as a high rate of rock dissolution and underground piercing cavity are capable of accelerating karst sinkholes. Four levels of formation lithology were classified (Yilmaz, 2007): (1) limestone, dolomite and dolomitic limestone, (2) siliceous rocks and limestone, (3) limestone conglomerate, and (4) siliceous rocks and siliceous mudstone. Using Eq. (2), the quantified index of formation lithology is calculated and presented in Table 4. The map of the four layers of formation lithology is depicted in Fig. 6.

4.2.2. Soil structure

Soil structure mainly refer to the permutation and combination of different types of lithological soil. It has commonly been accepted that changes in the permeability of soil and seepage deformation resistance can cause karst sinkholes. Therefore, the study area is divided into four types of soil structure (Lei et al., 1997; Zhu et al., 2000): (a) one-dual structure, (b) two-dual

Table 4
"Formation lithology" impact factor levels and quantification index.

Impact factor	Criteria			
	Level 1	Level 2	Level 3	Level 4
Formation lithology	Limestone, dolomite and dolomitic limestone	Siliceous rocks and limestone	Limestone	Conglomerate, siliceous rocks and siliceous mudstone
Quantified index	0.313	0.256	0.244	0.187

Table 5
"Soil structure" impact factor levels and quantification index.

Impact factor	Criteria			
	Level 1	Level 2	Level 3	Level 4
Soil structure	Silty clay	Silty clay, sand gravel	Silty clay, sand gravel, clay	Silty clay, silt, clay and sand gravel
Quantified index	0.396	0.256	0.203	0.145

structures, (c) multi-dual structures, and (d) mixed-dual structures. One-dual soil layer structures are commonly composed of silty clay. Two-dual structure layers consist of silty clay and sand gravel. Multi-dual soil layers consist of silty clay, sand gravel, and clay; and mixed-dual soil layer structures consist of silty clay, silt, clay, and sand gravel. Based on results obtained using Eq. (2), the quantification index of soil structure is presented in Table 5.

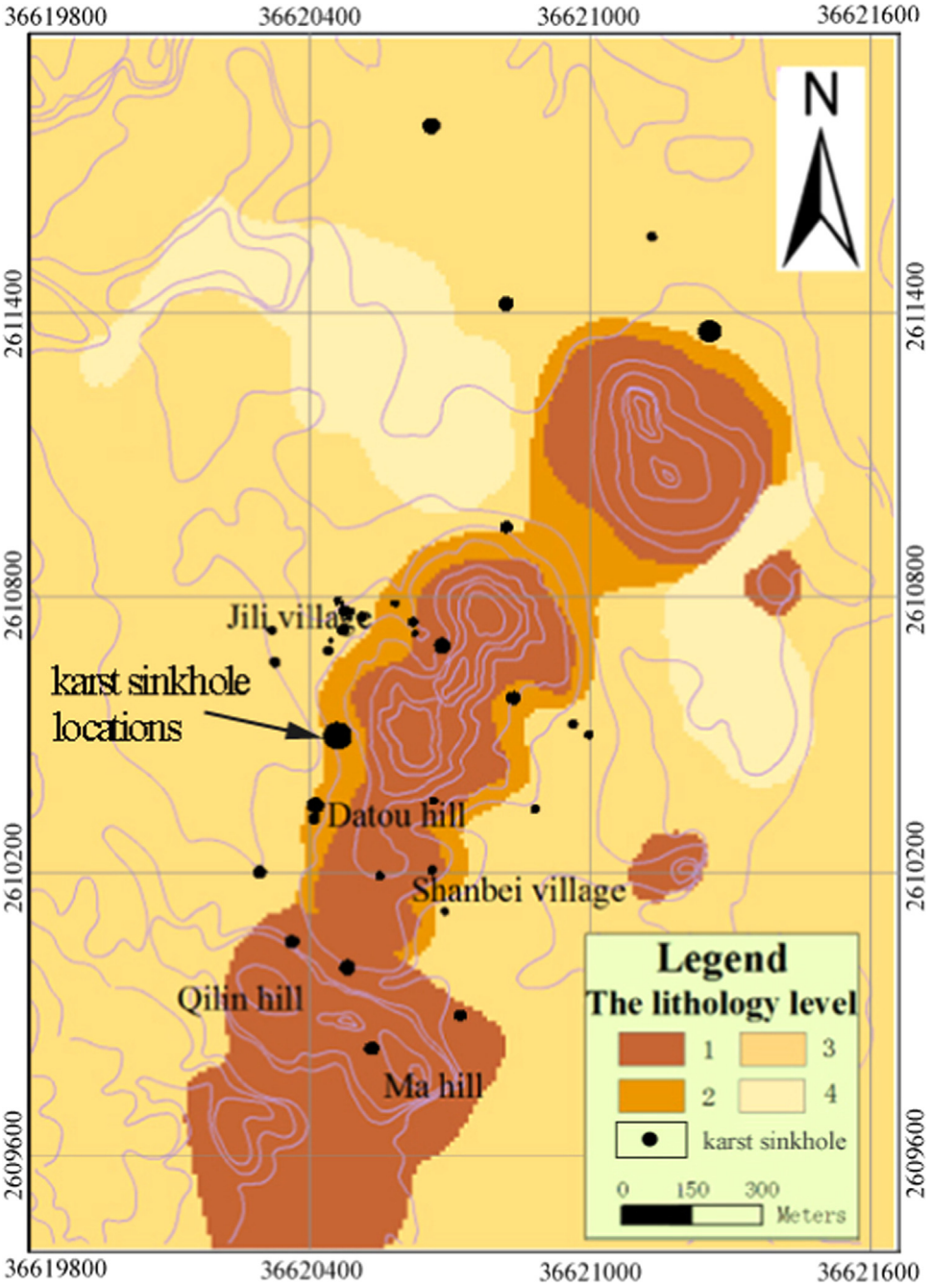

Fig. 6. Four types of formation lithology.

4.2.3. Profile curvature

The karst sinkholes in Jili Village occurred at the edges of the foothill, and surface water typically flows along the hillside and then converges in the sinkholes, contributing to second-time sinkholes. Seepage erosion and disintegration produced by groundwater are important causes of the formation and development of sinkholes. For this reason, this paper takes the profile curvature of surface terrain as an impact factor.

The profile curvature refers to the surface terrain slope. This paper uses the curvature to measure surface variations. The curvature is calculated using a second-order differential equation (Moore et al., 1993), which is a combination of the elevation gradient in both the horizontal and vertical plane. The mathematical model is expressed by

$$K_v = -\frac{p^2 r + 2pqs + q^2 t}{(p^2 + q^2)(1 + p^2 + q^2)^{\frac{3}{2}}} \quad (3)$$

where $p = \frac{\partial H}{\partial x}$, $q = \frac{\partial H}{\partial y}$ are the elevation gradients along the x, y directions, respectively, $r = \frac{\partial^2 H}{\partial x^2}$, $t = \frac{\partial^2 H}{\partial y^2}$ are the second-order differentials along the x, y direction, respectively, and $s = \frac{\partial^2 H}{\partial x \partial y}$ is the rate of elevation changes in the x and y directions.

In this paper, it adopts the method of converting the map of contour in a scale of 1:5000 to DEM. There are two steps involved in the data conversion from contour to DEM. First, the Triangular Irregular Network (TIN) is extracted through contour data (See Fig. 7), second the DEM is derived from TIN, and finally, the profile curvature (See Fig. 8) is calculated with DEM data. The

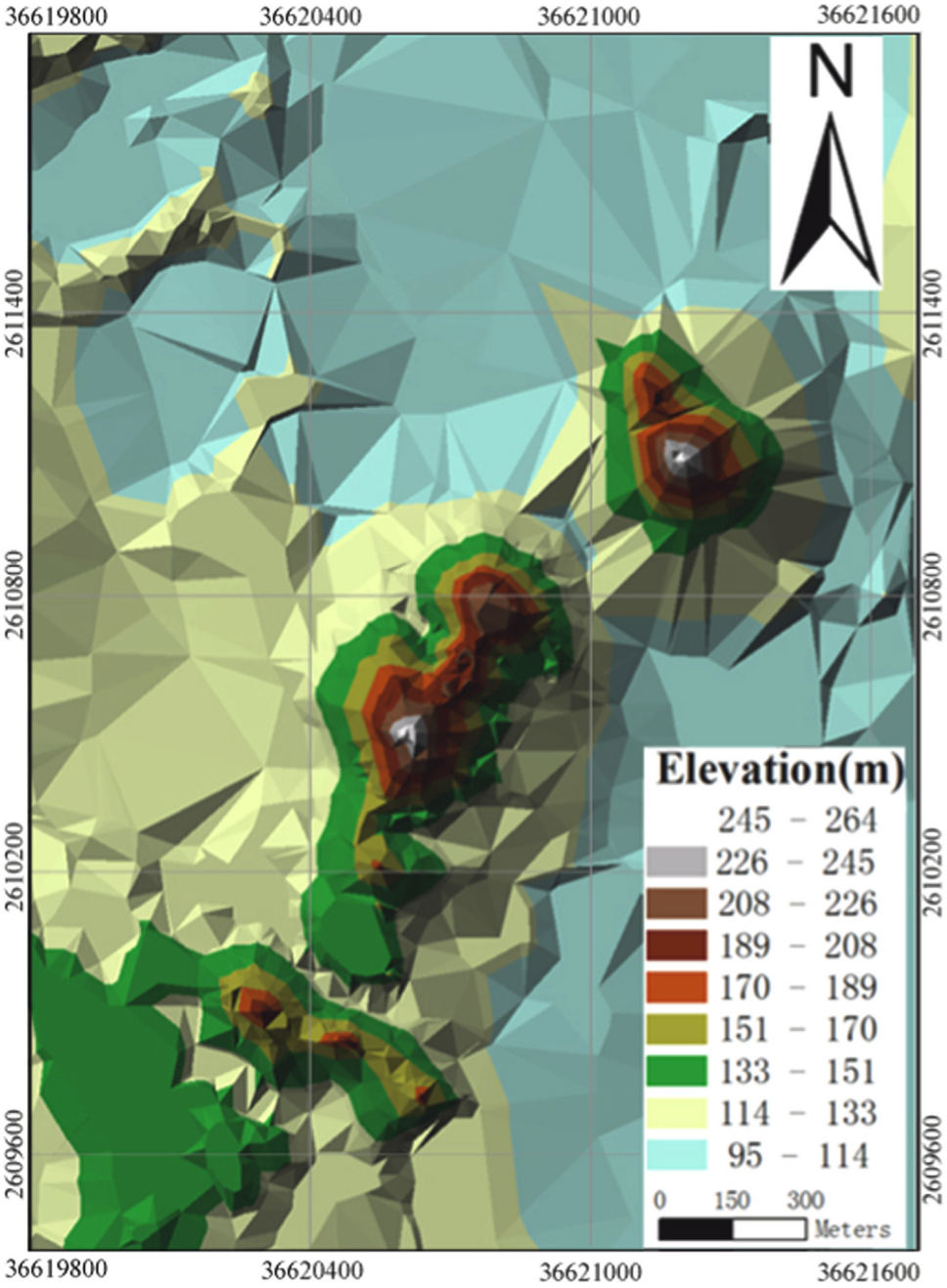

Fig. 7. Map of TIN.

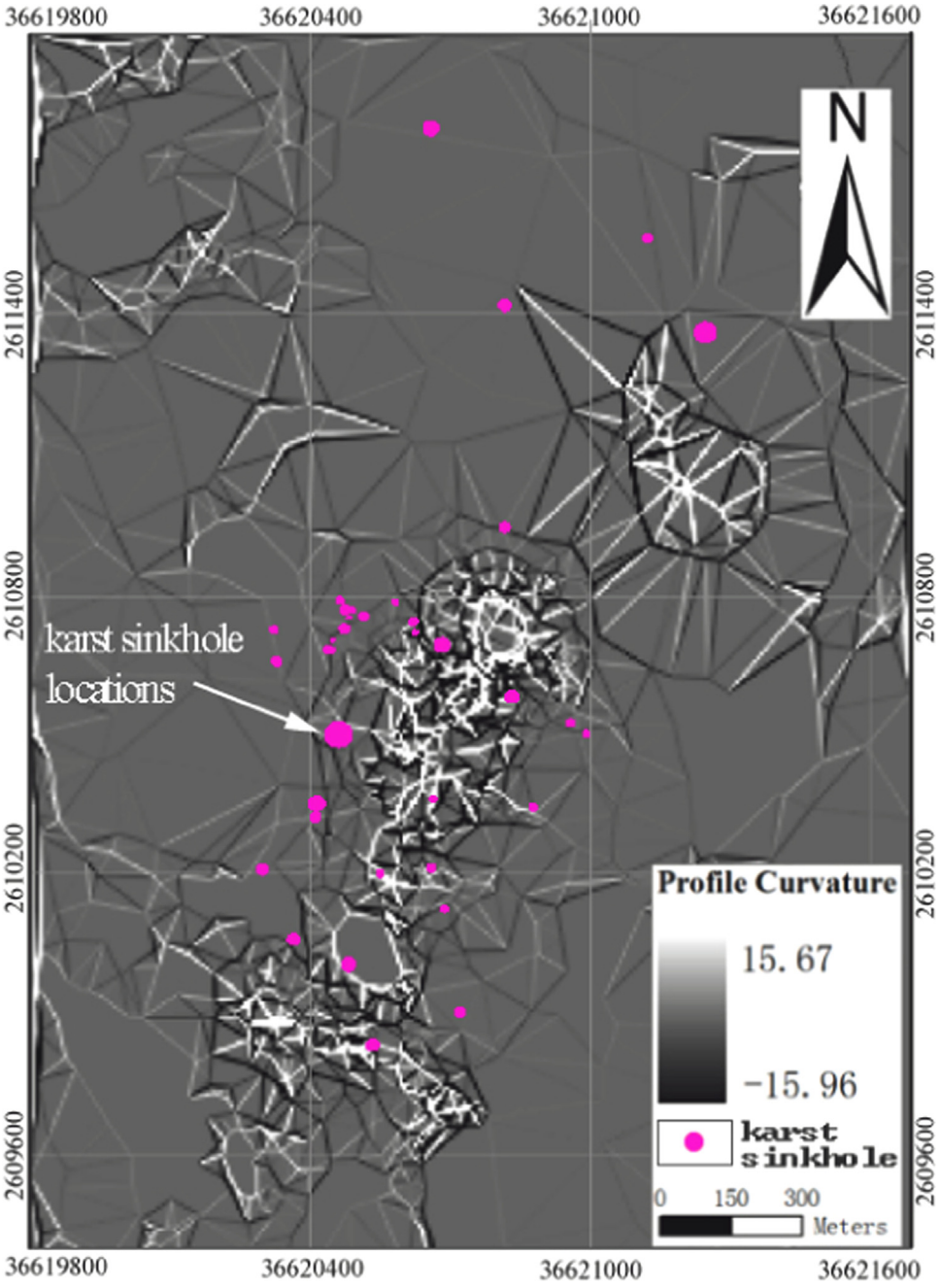

Fig. 8. Map of profile curvature.

Table 6
"Profile curvature" impact factor levels and quantification index.

Impact factor	Criteria			
	Level 1	Level 2	Level 3	Level 4
Profile curvature (deg.)	> 13	8–13	−5–8	< −5
Quantified index	0.198	0.419	0.243	0.140

study area is divided into four levels based on changes in slope. Based on Eq. (2) and Eq. (3) and according to the real situation of the study area and previous literature (Lulseged and Hiromitsu, 2005), the classification criteria and quantification index are as presented in Table 6.

4.2.4. Groundwater depth

Using an underground water level detector, groundwater depth data were obtained. The data reveal that the depth of groundwater in the study area is deeper than that in any other nearby areas. However, the depth of the groundwater is relatively shallow at the foothill. "The groundwater depth is sensitive to rainfall, which suggests that the rainfall controls the groundwater depth and is therefore a main external factor. According to the monitoring data from Laibin Weather Bureau, the total rainfall in the first nine months before karst sinkholes occurred in the study area is of 623.4 mm, while the rainfall ahead to one month of collapse is approximately 609.7 mm (see Fig. 9). Moreover, two days before the disaster, the rainfall lasted 12 h with a total rainfall of 442 mm.

Based on discussions in previous literature (Manda and Michael, 2006), the groundwater depth is classified into four levels: < 5 m, 5–10 m, 10–20 m, and greater than 20 m. Using Eq. (2), the

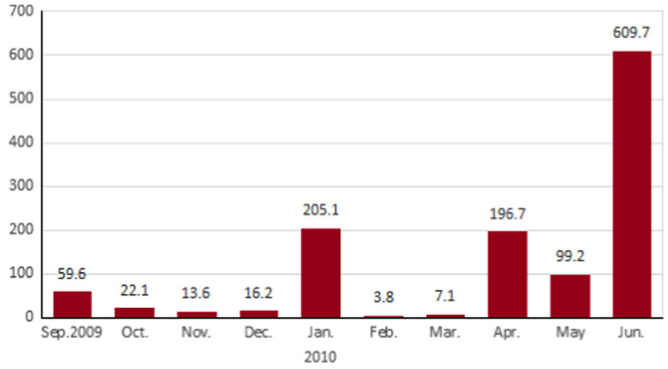

Fig. 9. Monthly mean rainfall of the study area (Laibin Weather Bureau).

Table 7
"Groundwater depth" impact factor levels and quantified index.

Impact factor	Criteria			
	Level 1	Level 2	Level 3	Level 4
Groundwater depth (m)	< 5	5–10	10–20	> 20
Quantified index	0.415	0.225	0.183	0.177

quantification index of the groundwater depth is calculated and presented in Table 7.

4.2.5. Fluctuation of groundwater level

The groundwater fluctuation layer is obtained by the method of spatial interpolation to the data obtained by an underground water level detector, and thus the observation period of this data perfectly matches the groundwater depth data.

A river named Hongshui River, which is located 25 km north of Jili Village, is the groundwater drainage of the study area. The annual average flow of Hongshui River is nearly 2000 m^3/s; the maximum average flow is about 15,000 m^3/s; the minimum average flow is about 286 m^3/s; and the annual runoff is approximately 608.3×10^8 m^3 (Laibin hydrological monitoring station).The groundwater depth observations show that the fluctuation of the groundwater level in the study area is greater than that in the other areas. The fluctuation of the groundwater has a stronger effect on the karst sinkholes than the groundwater level does. The fluctuation of groundwater is classified into four levels (Galve et al., 2008; Kyriaki et al., 2013): < 3 m, 3–5 m, 5–10 m, and greater than 10 m. Based on Eq. (2), the quantification index of the groundwater fluctuation levels are as shown in Table 8, and a map describing the extent of groundwater level fluctuations is depicted in Fig. 10.

4.2.6. Percolation rate of soil

As is usually the case, the soil near the fault is easily cracked. In addition, strong weathering generally occurs in the fault intersection area, which leads to a relatively high percolation rate of soil near the fault. Based on the experts' experiences of the Laibin hydrological monitoring station and reference of Ha et al. (2009), the impact factor of "Percolation rate of soil" was classified into three levels. Using Eq. (2), the quantification index of the percolation rate of soil is calculated and presented in Table 9.

Table 8
"Groundwater fluctuation" impact factor levels and quantification index.

Impact factor	Criteria			
	Level 1	Level 2	Level 3	Level 4
Fluctuation of ground water level (m)	< 3	3–5	5–10	> 10
Quantified index	0.066	0.153	0.406	0.375

4.2.7. Degree of karst development

The degree of karst development is one of the most important factors affecting karst sinkholes. The degree of karst development is assessed by a ground penetrating radar (GPR) instrument, using high density resistivity and drilling data (see Fig. 11), and is divided into four levels. Based on Eq. (2), the quantification index of the degree of karst development is as presented in Table 10.

4.2.8. Distance from fault

The study area contains nine faults. It is observed that almost all sinkholes have occurred in the buffer area, which is created using a distance of 250 m along fault centerline. The analysis also shows that (1) many sinkholes have occurred in the cross-hatched area and (2) a distinct linear relationship between the distribution density of sinkholes and the distance from the fault exists. The distance away from fault is divided into three levels: < 50 m, 50–100, and 100–250 m. Based on Eq. (2), the quantification index of distance from the fault is as presented in Table 11. A line buffer located 250 m from the fault centerline is created and depicted in Fig. 12. It can be indicated from Fig. 12 that three levels are enough to reveal the impact factor of distance from fault to karst sinkholes.

4.2.9. Distance from traffic routes

There are three main traffic routes across the study area, the Gui-Lai expressway, the Liu-Nan expressway, and a railway. They are located in the east, west and north direction of the study area respectively, and the three traffic routes form a semicircle that half-encloses the study area. Based on previous literature (Kyriaki et al., 2013), the distances from the sinkholes are categorized into four levels: < 100 m, 100–400 m, 400–600 m and > 600 m. Based on Eq. (2), the quantification index of distance away from the traffic route is as presented in Table 12.

4.2.10. Overburden thickness

The overburden thickness refers to the soil thickness over cap rock. The depths of overburden thickness were acquired by geophysical prospecting methods and Kriging interpolation method in ArcGIS software. Based on previous literature (Gómez-Ortiz and Martín-Crespo, 2012), overburden thicknesses are classified into four levels in the study area: < 5 m, 5–10 m, 10–25 m and > 25 m. Using Eq. (2), the quantification index is calculated and presented in Table 13.

4.3. Spatial analysis using a logistic model

4.3.1. Logistic regression model

Logistic regression, which was first proposed by Verhulst in 1845, can be expressed by

$$P = \frac{e^{\beta_0+\beta_1 x_1+\ldots+\beta_n x_n}}{1+e^{\beta_0+\beta_1 x_1+\ldots+\beta_n x_n}} \quad (4)$$

Where P is the sensitive probability, β_i ($i=1, 2\ldots n$) are the logistic regression coefficients, β_0 is a constant, and x_i ($i=1, 2\ldots n$) are the independent variables.

To determine which variables (impact factors) significantly affect karst sinkholes, this paper first selects initial impact factors, computes the coefficients using the logistic model, and later deletes coefficients (impact factors) that make only slight contributions to karst sinkholes. The same computation is then repeated through iteration until all coefficients are calculated. A flowchart of this process is shown in Fig. 13 and consists of the following steps:

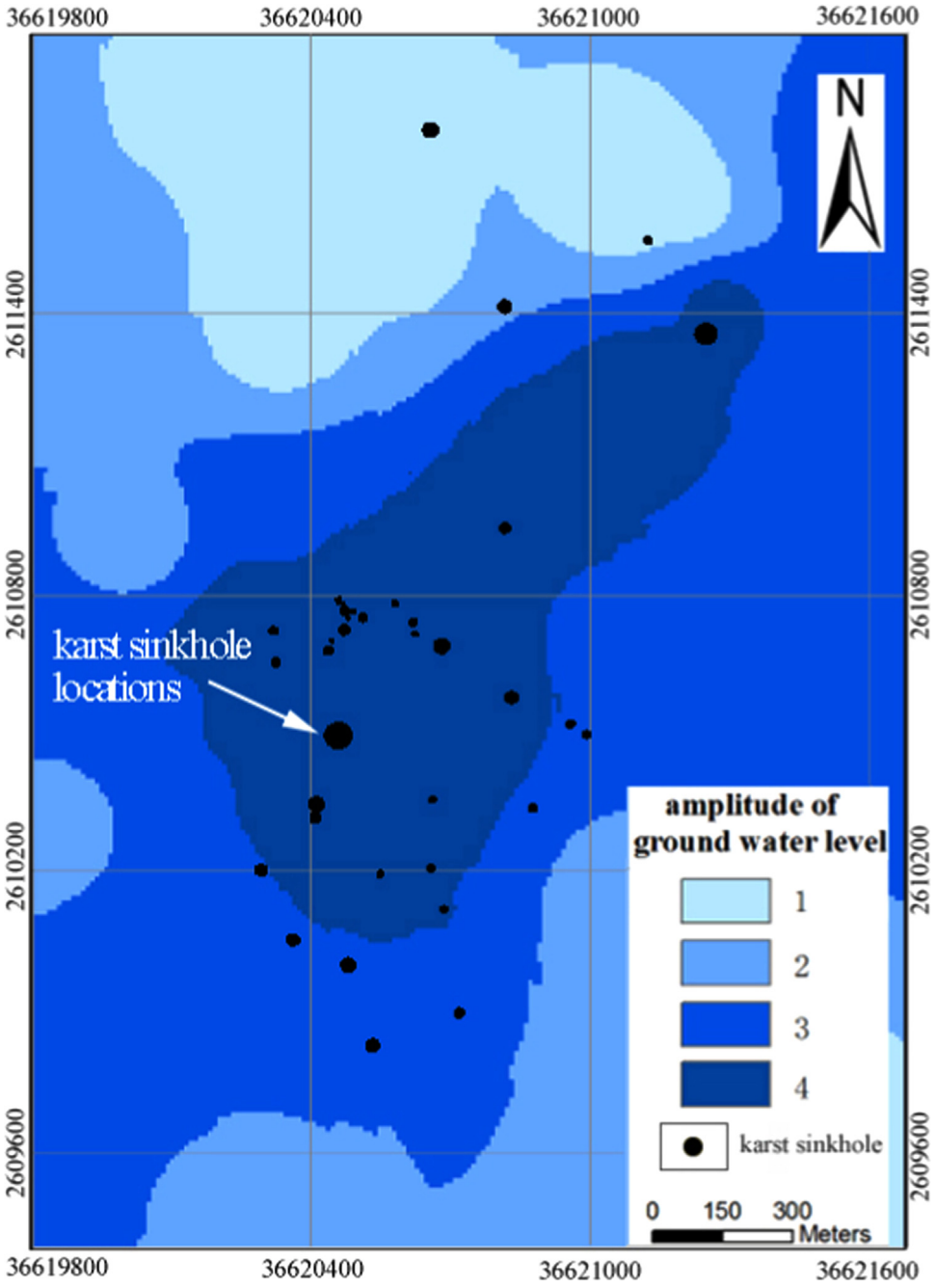

Fig. 10. Fluctuation of ground water level.

Table 9
"Percolation rate of soil" impact factor levels and quantified index.

Impact factor	Criteria		
	Level 1	Level 2	Level 3
Percolation rate of soil cm/s	$>3\times10^{-3}$	3×10^{-4}–3×10^{-3}	$<3\times10^{-4}$
Quantified index	0.435	0.356	0.209

1. *Step 1:* initially choose reasonable impact factors that are considered to contribute to sinkholes;
2. *Step 2:* subdivide the impact factors into secondary classes, associated with their values;
3. *Step 3:* rasterize all layers and generate a uniform grid size;
4. *Step 4:* employ the logistic model to calculate the coefficients, $\beta_1 \ldots \beta_n$, based on the collected data, and establish a logistic model;
5. *Step 5:* delete the impact factors whose contribution to karst sinkholes are small, and re-compute the coefficient of the LRM;
6. *Step 6:* repeat *Step 4* and *Step 5*, until all coefficients are calculated;
7. *Step 7:* use the computed coefficients to establish an LRM for classifying the levels of susceptible areas.

The data used in the logistic model are randomly selected from the collected data set. A total of 115 sinkholes "pixels" and 480 non-occurring sinkholes "pixels" (each pixel represents an area of 5×5 m^2) are employed in this study. The data are input into the logistic model for regression computation. During the iterations, it

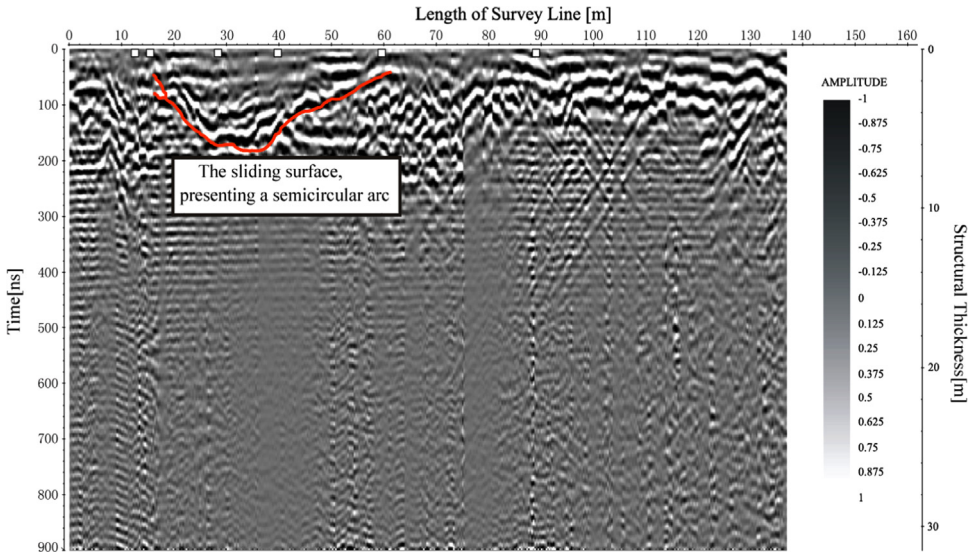

Fig. 11. Line profile of GPR (from Geological Environment Monitoring Station of Guangxi).

Table 10
"Degree of karst development" impact factor levels and quantification index (Note: High-developed=Line karst rate >10%; Mid-developed=Line karst rate 5–10%; Low-developed=Line karst rate 1–5%; No development=Line karst rate <1%.).

Impact factor	Criteria			
	Level 1	Level 2	Level 3	Level 4
Development degree of karst	High-developed	Mid-developed	Low-developed	No development
Quantified index	0.241	0.223	0.358	0.178

is observed that the sigma error of the coefficient for the impact factor "distance between the traffic routes and the sinkholes area" is greater than 0.05, which means that it will contribute little to the karst sinkholes. Therefore, it is eliminated from the next iteration. This computation is repeated until all sigma errors of impact factors are less than a given threshold (0.05). Finally, 9 coefficients $\beta_i (i = 1, 2, \ldots, 9)$ plus a constant, β_0, are solved for. With the solved coefficients, the logistic model is established based on Eq. (5), and the corresponding factors are listed in Table 14. These factors are considered contributors to karst sinkholes in the study area and are thus referred to as *impact factors*.

Table 11
"Distance from fault" impact factor levels and quantification index.

Impact factor	Criteria		
	Level 1	Level 2	Level 3
Distance from fault (m)	<50	50–100	100–250
Quantified index	0.509	0.323	0.168

probabilities are 0.823–0.964, 0.716–0.823, 0.522–0.716, 0.076–0.522, and 0–0.076, respectively. The corresponding five classes of sinkhole areas are mapped in Fig. 14a. The results of statistical analysis of each class of susceptible area are listed in Table 16. As shown in the table, the percentages of the sinkhole area over the entire study area are 0% for "non-susceptible", 6.2% for "low", 25.0% for "moderate", 27.6% for"high" and 41.2% for "very high." It can therefore be concluded that the higher the susceptibility level is, the greater the sinkhole occurrence probability becomes.

5. Precision assessment and field verification

To verify the precision achievable when using the logistic regression method, this paper uses the Sridevi Jadi model (Jadi, 1997), i.e.,

$$P = \frac{e^{-4.102+0.211x_{1j}+0.310x_{2j}+0.087x_{3j}+0.155x_{4j}+0.206x_{5j}+0.198x_{6j}+0.356x_{7j}-0.264x_{8j}-0.286x_{10j}}}{1 + e^{-4.102+0.211x_{1j}+0.310x_{2j}+0.087x_{3j}+0.155x_{4j}+0.206x_{5j}+0.198x_{6j}+0.356x_{7j}-0.264x_{8j}-0.286x_{10j}}} \quad (5)$$

4.3.2. Identification of susceptible areas

The probability of each pixel in the study area is calculated using Eq. (5), in which the quantification indices of the impact factors are employed. The magnitude of probability indicates the probability of karst sinkholes occurrence (Table 15). The study area is categorized into five classes of susceptibility according to the real situation and previous literature (Yilmaz, 2007): very high susceptible area, high susceptible area, moderate susceptible area, low susceptible area, and non-susceptible area; the corresponding

$$P' = \frac{KS}{S}\left(1 - \frac{K - KS}{N - S}\right)^{\frac{1}{3}} \quad (6)$$

where N is the total number of pixel; S is the number of pixels corresponding to existing sinkholes; K is a combination of the unit numbers of very high susceptible areas, high susceptible areas, and moderate susceptible areas; KS is the total number of pixels corresponding to sinkholes of medium, high, and very high susceptible areas, which corresponds to the probability of karst sinkhole

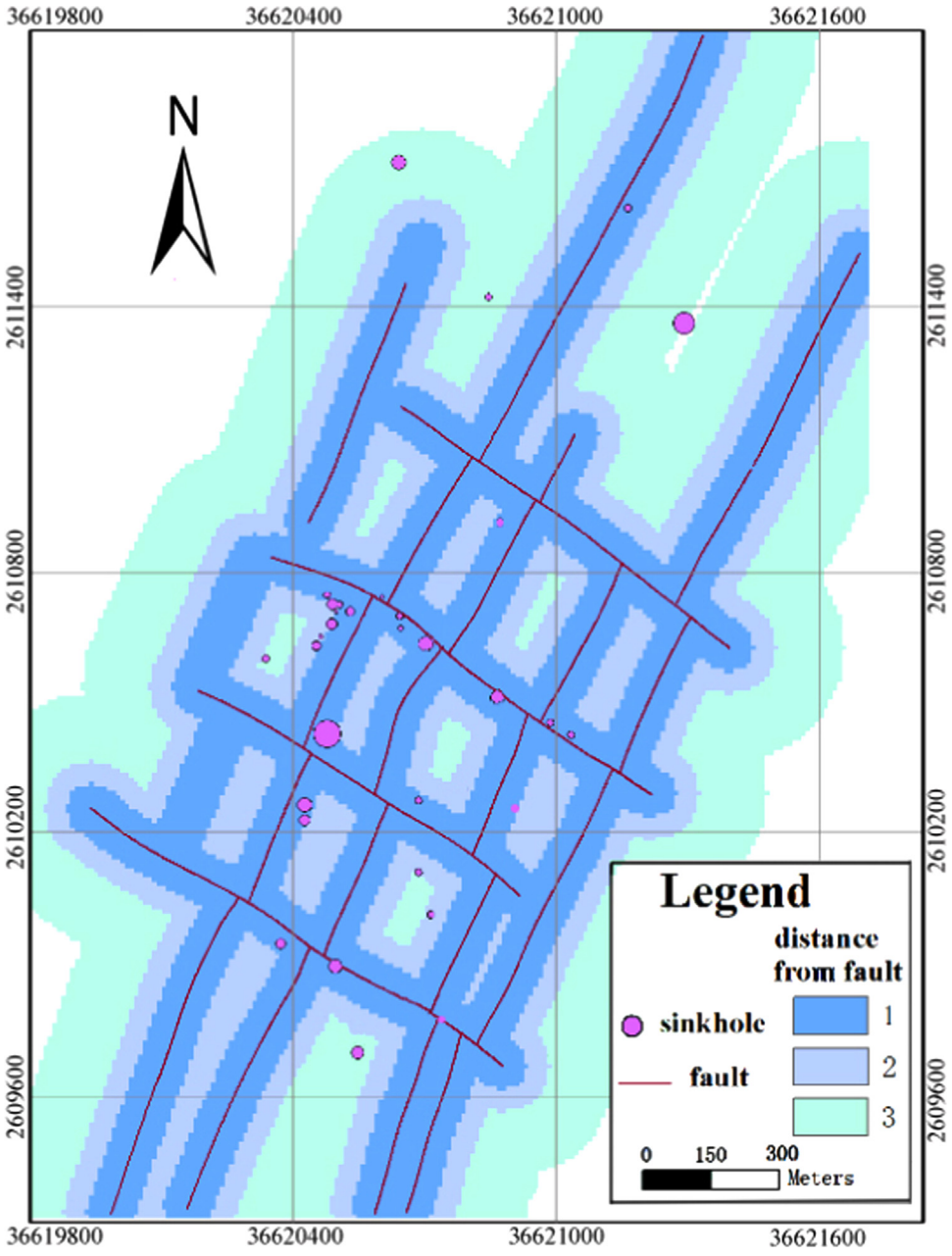

Fig. 12. Distance from fault.

Table 12
"Distance from the traffic route" impact factor levels and quantification index.

Impact factor	Criteria			
	Level 1	Level 2	Level 3	Level 4
Distance from the traffic route(m)	< 100	100–400	400–600	> 600
Quantified index	0.241	0.223	0.358	0.178

Table 13
"Overburden thickness" impact factor levels and quantification index.

Impact factor	Criteria			
	Level 1	Level 2	Level 3	Level 4
Overburden thickness (m)	< 5	5–10	10–25	> 25
Quantified index	0.300	0.313	0.289	0.098

occurrence. For the pixels considered in the study area, N is 48,100, S is 192, KS is 180, and K is 23,243. Based on Eq. (6), 73% prediction accuracy is achieved in the study area. This value demonstrates that our prediction is reliable in theory (Galve et al., 2009a,b; Li et al., 2011).

To further evaluate the accuracy of the method proposed in this paper, we conducted a field investigation. The field verification was carried out just to confirm if there were sinkholes in the area, the size and number, and the geological structure etc. the detailed field verification data is shown in Table 17.

Based on the field investigation results, it is demonstrated that the majority of sinkholes are mainly distributed in the very high susceptible and high susceptible areas along Datou Hill and foothills (Fig. 14). The geological characteristics corresponding to each susceptibility level considered in this study are as follows:

(1) *Very high susceptible area:* most karst sinkholes are mainly located in the very high susceptible and high susceptible

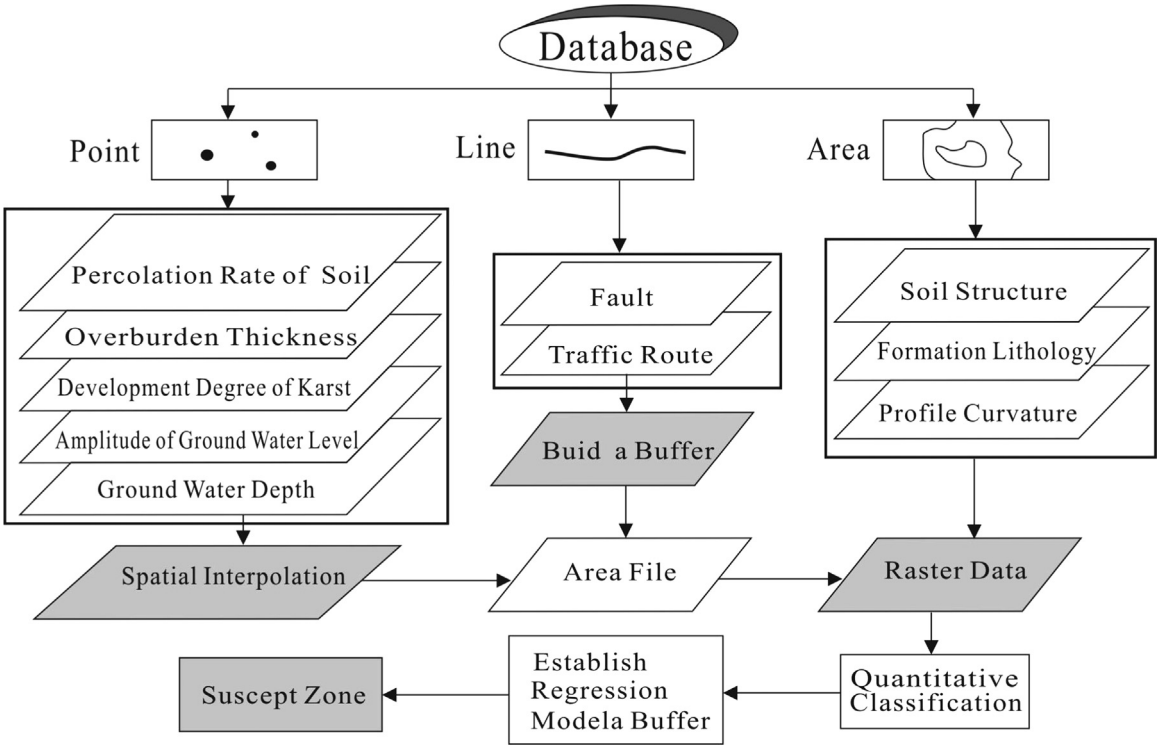

Fig. 13. Flowchart describing process of identifying impact factors using the logistic model.

Table 14
The coefficients regressed using the logistic model.

Factors	formation lithology	soil structure	profile curvature	groundwater depth	ground water level
Coefficients	$\beta_1=0.211$	$\beta_2=0.310$	$\beta_3=0.087$	$\beta_4=0.155$	$\beta_5=0.206$
Factors	Percolation rate of soil	Degree of karst development	Distance from fault	Distance from the traffic route	Overburden thickness
Coefficients	$\beta_6=0.198$	$\beta_7=0.356$	$\beta_8=-0.264$	$\beta_9=$eliminated	$\beta_{10}=-0.286$

Table 15
Probability of each susceptibility level.

Susceptibility Level	Very high	High	Moderate	Low	Non-susceptible
Probability (P)	0.823–0.964	0.716–0.823	0.522–0.716	0.076–0.522	0–0.076

areas, where the geological structure is very complex; karst is well developed, and the integrity of rock mass is poor. The karst sinkholes occurred in a single form (see Fig. 14c and d).

(2) *High susceptible area:* this area includes areas where many geological faults are located. The siliceous rocks in this area have been weathered to a brecciated texture. Flexure and fractures further formed loose rocks and soil mixtures. A lot of crack appeared on the ground (see Fig. 14f and g).

(3) *Moderate susceptible area:* this area includes regions where sinkholes previously occurred, but these sinkholes were smaller than those in other areas. The distribution is zonal and punctuated, and the level of karst development is intermediate (see Fig. 14h).

(4) *Low susceptible area:* this area includes regions where the terrain is flat and the activity of groundwater is gentler (see Fig. 14b).

(5) *Non-susceptible area:* this area includes regions where the geological condition is very good. The karst is not developed, the siliceous rocks are hard and thick, and the area is located far from faults (see Fig. 14e).

Based on the above analysis, it is suggested that residents in the very high susceptible and high susceptible areas should be relocated.

6. Conclusions

This paper conducts a geospatial analysis on the basis of ten types of geospatial data for karst sinkhole susceptibility in Jili, a small village in southwest of China, which has experienced the first-time sinkholes. The ten types of geospatial data are quantitated and then managed using ArcGIS software. The Logistic Regression model is applied to select the significant contribution factors to the sinkhole. Nine out of the ten factors, including formation lithology, soil structure, profile curvature, groundwater depth, ground water level, percolation rate of soil and degree of karst development, the distance from fault, and overburden thickness were identified to be significantly related to karst sinkholes occurrences.

In the regression coefficient results of Logistic model based on hydrogeological information and GIS, it was proved that the high-hazard karst susceptibility areas were located along Datou Hill and foothills, which are consistent with the results of field investigation. And the preliminary susceptibility models obtained and the

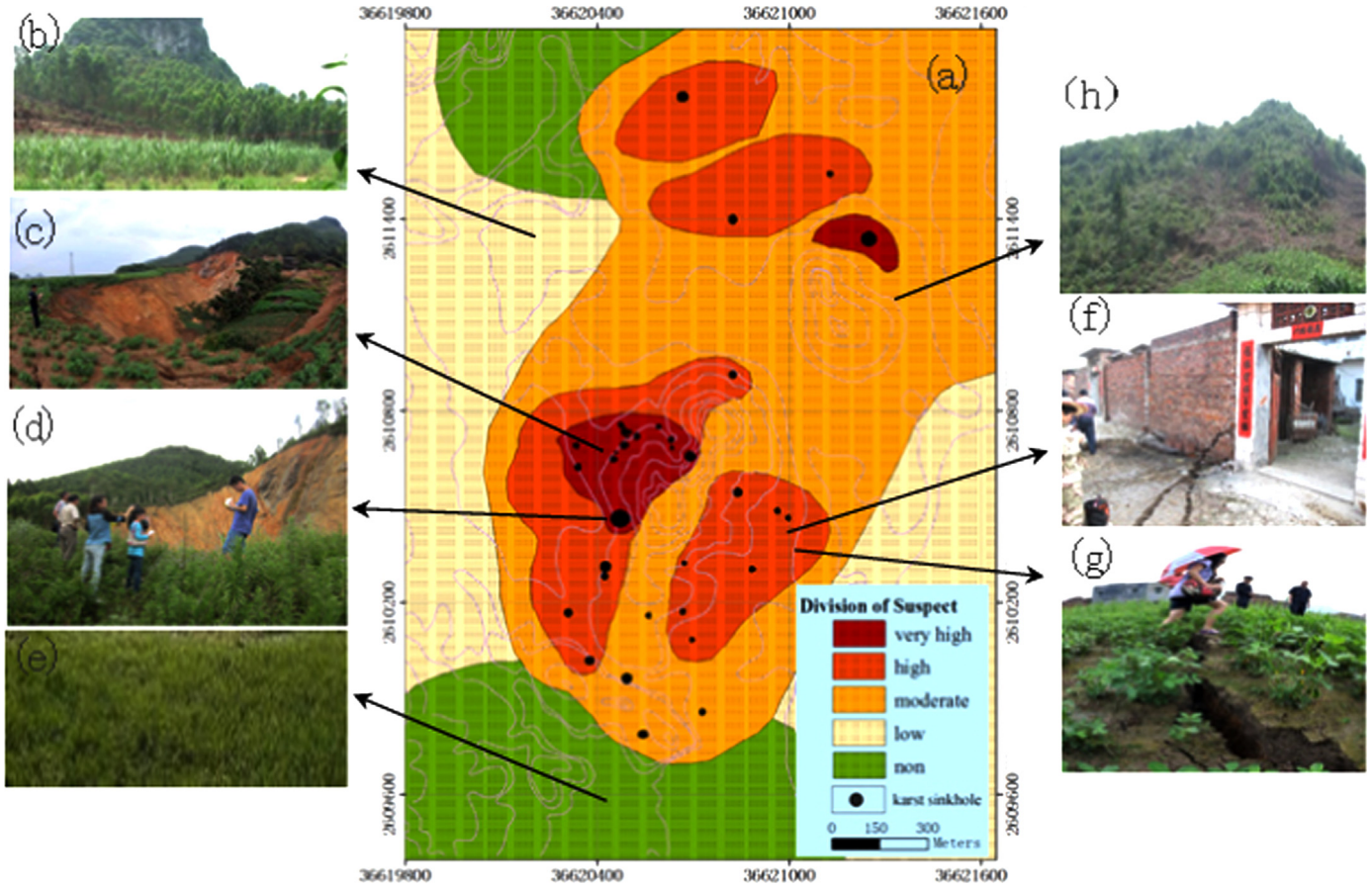

Fig. 14. Classification and the recognized susceptible areas and their field verification.

Table 16
Division of susceptibility.

Susceptibility level	Partition pixel numbers	Percentage (%)	Pixel numbers of sinkholes	Percentage of sinkholes (%)
Very high	1351	2.8	79	41.2
High	7030	14.6	53	27.6
Moderate	17,584	36.6	48	25.0
Low	13,579	28.2	12	6.20
Non-susceptible	8556	17.8	0	0

Table 17
The detailed field verification data.

Susceptibility level area	Sinkholes number	Sinkholes size	Geological characteristics
Very high	13	Diameter: 40–70 m Visible depth: 10–30 m	Well-developed karst; single karst sinkholes
High	13	Diameter: 30–60 m Visible depth: 5–20 m	Geological faults located weathered siliceous rocks a lot of crack
Moderate	4	Diameter: 2–20 m Visible depth: 5–10 m	Intermediate-developed karst small sinkholes, zonal and punctuated distribution
Low	0	–	Flat terrain gentler groundwater activity
Non-susceptible	0	–	No-developed karst far from faults hard and thick siliceous rocks

validation show that it is possible to produce reasonably satisfactory predictions on the spatial distribution of future sinkholes in the study area. The validated models suggest that the distribution of around 73% of the future sinkholes might be anticipated with the 17% of the area with the highest susceptibility. Moreover, about 46% of the area could be considered as safe. These predictions were tested by means of independent validation, which might be used as a reference by the local authorities to make decisions whether or not residents living within the sinkhole areas should move.

Acknowledgments

This paper is financially supported by the National Natural Science Foundation of China under Grant numbers 41431179 and 41162011, GuangXi Governor Grant under approval number 2010-169, GuangXi Grand Natural Science Foundation under Grant number 2015GXNSFDA139032, Guangxi Science & Technology Development Program under the Contract number GuiKeHe 14123001-4, and GuangXi Key Laboratory of Spatial Information and Geomatics Program (Contract nos. GuiKeNeng 110310801, 120711501, 130511401, 130511409 and 130511415), the "BaGui Scholars" program of the provincial government of Guangxi.

Appendix A. Supporting information

Supplementary data associated with this article can be found in the online version at http://dx.doi.org/10.1016/j.cageo.2016.02.001. These data include Google maps of the most important areas described in this article.

References

Aronn, K., 1991. Stepwise overlay approach for utilizing a GIS with a soil moisture accounting model. ITC J., 17–18.
Ayalew, L., Yamagishi, H., 2005. The application of GIS-based logistic regression for landslide susceptibility mapping in the Kakuda–Yahiko Mountains, Central Japan. Geomorphology 65, 15–31.
Bathrellos, G.D., Kalivas, D.P., Skilodimou, H.D., 2009. GIS-based landslide susceptibility mapping models applied to natural and urban planning in Trikala, Central Greece. Estudios Geol. 65 (1), 49–65.
Carbonel, D., Rodríguez-Tribaldos, V., Gutiérrez, F., Galve, J.P., Guerrero, J., Zarroca, M., Roqué, C., Linares, R., McCalpin, J.P., Acosta, E., 2015. Investigating a damaging buried sinkhole cluster in an urban area (Zaragoza city, NE Spain) integrating multiple techniques: geomorphological surveys, DInSAR, DEMs, GPR, ERT, and trenching. Geomorphology 229, 3–16.
Chen, J.N., 2008. Application of GIS technology to comprehensive management of surface subsidence area due to underground coalmining. Coal Sci. Technol. 36 (12), 82–85 (in Chinese).
Chen, Z.H., Jin, M.G., 1992. Geographic information system and water resources system analysis, simulation and decision making. Proc. Hydrogeol. Eng. Geol., 60–64.
Choi, J.K., Kim, K.D., Lee, S., Won, J.S., 2010. Application of a fuzzy operator to susceptibility estimations of coal mine subsidence in Taebaek City, Korea. Environ. Earth Sci. 59 (5), 1009–1022.
Deborah, J.G., Waleed, A.A., 2002. Stability charts for predicting sinkholes in weakly cemented sand over karst limestone. Eng. Geol. 65, 179–184.
Frumkin, A., 2013. New developments of karst geomorphology concept. Geomorphology 6, 1–13.
Farrant, A.R., Cooper, A.H., 2008. Karst geohazards in the UK: the use of digital data for hazard management. Q. J. Eng. Geol. Hydrogeol. 41, 339–356.
Galve, J.P., Bonachea, J., Remondo, J., et al., 2008. Development and validation of sinkhole susceptibility models in mantled karst settings. A case study from the Ebro valley evaporite karst (NE Spain). Eng. Geol. 99, 185–197.
Galve, J.P., Gutiérrez, F., Remondo, J., Bonachea, J., Lucha, P., Cendrero, A., 2009a. Evaluating and comparing methods of sinkhole susceptibility mapping in the Ebro Valley evaporate karst (NE Spain). Geomorphology 111, 160–172.
Galve, J.P., Gutiérrez, F., Lucha, P., Guerrero, J., Bonachea, J., Remondo, J., Cendrero, A., 2009b. Probabilistic sinkhole modelling for hazard assessment. Earth Surf. Process. Landf. 34 (3), 437–452.
Galve, J.P., Castañeda, C., Gutiérrez, F., Herrera, G., 2015. Assessing sinkhole activity in the Ebro Valley mantled evaporite karst using advanced DInSAR. Geomorphology 229, 30–44.
Gao, Y., Alexander Jr., E.C., Barnes, R.J., 2005. Karst database implementation in Minnesota: analysis of sinkhole distribution. Environ. Geol. 47 (8), 1083–1098.
Gómez-Ortiz, T., Martín-Crespo, 2012. Assessing the risk of subsidence of a sinkhole collapse using ground penetrating radar and electrical resistivity tomography. Eng. Geol. 149–150, 1–12.
Gutiérrez, F., Mozafari, M., Carbonel, D., Gómez, R., Raeisi, E., 2015. Leakage problems in dams built on evaporites. The case of La Loteta Dam (NE Spain), a reservoir in a large karstic depression generated by interstratal salt dissolution. Eng. Geol. 185, 139–154.
Gutiérrez-Santolalla, F., Gutiérrez-Elorza, M., Marín, C., Maldonado, C., Younger, P.L., 2005. Subsidence hazard avoidance based on geomorphological mapping in the Ebro River valley mantled karst terrain (NE Spain). Environ. Geol. 48, 370–383.
Ha, S., Kim, J.G., Kim, N., 2009. Classification of hydrologic soil groups of soil originated from limestone by assessing the rates of infiltration and percolation. Korean J. Soil Sci. Fertil. 42 (2), 103–109.
Hyun, J.O., Saro, L., 2010. Assessment of ground subsidence using GIS and the weights-of-evidence model. Eng. Geol. 115, 36–48.
Işık, Y., 2007. GIS based susceptibility mapping of karst depression in gypsum:A case study from Sivas basin (Turkey). Eng. Geol. 90, 89–103.
Jadi, Sridevi, 1997. Statistical models of the slope instability. World Geol. 16 (1), 83–88.
Kaufmann, O., Quinif, Y., 2002. Geohazard map of cover-collapse sinkholes in the 'Tournaisis' area, southern Belgium. Eng. Geol. 65, 117–124.
Kim, K.D., 2006. Prediction and Verification of Ground Subsidence at Abandoned Underground Coal Mine Area Using GIS: Examples From Samcheok City, KangwonDo, Korea (Doctoral Dissertation Thesis). Yonsei University, Seoul.
Kim, K.D., Lee, S., Oh, H.J., 2009. Prediction of ground subsidence in Samcheok City, Korea using artificial neural networks and GIS. Eng. Geol. 58 (1), 61–70.
Kranjc, A., 2013. Classification of closed depressions in carbonate karst. Geomorphology 6, 104–111.
Kyriaki, P.V., George, D.B., Hariklia, D.S., George, K., Kostas, M., 2013. Karst collapse susceptibility mapping considering peak ground acceleration in a rapidly growing urban area. Eng. Geol. 158, 77–88.
Lamelas, M.T., Marinoni, O., Hoppe, A., de la Riva, J., 2008. Doline probability map using logistic regression and GIS technology in the central Ebro Basin (Spain). Environ. Geol. 54, 963–977.
Lee, S., Oh, H.J., Kim, K.D., 2010. Statistical spatial modeling of ground subsidence hazard near an abandoned underground coal mine. Disaster Adv. 3 (1), 11–13.
Lee, S., Min, K., 2001. Statistical analysis of landslide susceptibility at Yongin, Korea. Environ. Geol. 40, 1095–1113.
Lee, S., Sambath, T., 2006. Landslide susceptibility mapping in the Dammrei Romel area, Cambodia using frequency ratio and logistic regression models. Environ. Geol. 50, 846–855.
Lei, M.T., Jiang, X.Z., Li, Y., 1997. Sinkhole evaluation system and its application—taking the sinkholes in Tangshan city for example. Carsologica Sin. 16 (2), 97–104 (In Chinese).
Li, J., Zhou, C.H., 2003. Appropriate grid size for terrain based landslide risk assessment in Lantau Island, Hong Kong. J. Remote Sens. 7 (2), 86–93.
Li, Z.C., 1984. Main results of regional geological survey in Guangxi. Reg. Geol. China 9, 4–7 (In Chinese).
Li, X., Zhou, S., Xu, G., 2011. GIS-based risk assessment to karst susceptibility of Shenzhen Universiade Center (China). Procedia Environ. Sci. 10, 1389–1395.
Liu, S., 2013. The study of areas prone to geological disasters in Guangxi based on ArcGIS (Master Dissertation Thesis). Guangxi Teachers Education University, Guangxi, pp. 1–9 (In Chinese).
Lulseged, A., Hiromitsu, Y., 2005. The application of GIS-based logistic regression for landslide susceptibility mapping in Kakuda-Yahiko Mountains, Central Japan. Geomorphology 65 (2), 15–31.
Mancini, F., Stecchi, F., Gabbianelli, G., 2009. GIS-based assessment of risk due to salt mining activities at Tuzla (Bosnia and Herzegovina). Eng. Geol. 109 (3–4), 170–182.
Manda, K.A., Michael, R.G., 2006. Identifying and characterizing solution conduits in karst aquifers through geospatial (GIS) analysis of porosity from borehole imagery: An example from the Biscayne aquifer, South Florida (USA). Adv. Water Resour. 29, 383–396.
Mejia-Nabarro, M., Luis, A.G., 1996. Natural hazard and risk assessment using decision support systems. Environ. Eng. Geosci. 2, 299–324.
Moore, I.D., Gessler, P.E., Nielsen, G.A., Peterson, G.A., 1993. Soil attribute prediction using terrain analysis. Soil Sci. Soc. Am. J. 57 (2), 443–452.
Raghu, D., 1984. Sinkhole risk analysis for a selected area in Warren County, New Jersey. In: Proceedings of the First Multidisciplinary Conference on Sinkholes and the Environmental Impacts of Karst. Orlando, Florida.
Shi, J., Liang, C.M., 1997. A preliminary study on the relation between karst collapse and groundwater in Guilin. Geol. Hazard Control 8, 88–97 (In Chinese).
Tao, S., Hu, D., Zhao, W., Fan, Y., Wang, Z., 2010. Susceptibility assessment of secondary landslides triggered by earthquakes: A case study of northern Wenchuan. Geogr. Res. 29 (9), 1594–1605 (In Chinese).
Taheri, K., Gutiérrez, F., Mohseni, H., Raeisi, E., Taheri, M., 2015. Sinkhole susceptibility mapping using the analytical hierarchy process (AHP) and magnitude–frequency relationships: a case study in Hamadan province, Iran. Geomorphology 234, 64–79.
Van Westen, C.J., 2013. Remote sensing and GIS for natural hazards assessment and disaster risk management. Geomorphology 3, 259–298.
Verachtert, E., Eeckhaut, M.V.D., Poesen, J., Govers, G., Deckers, J., 2011. Prediction of spatial patterns of collapsed pipes in loess-derived soils in a temperate humid climate using logistic regression. Geomorphology 130, 185–196.

Waele, J.D., Gutiérrez, F., Parise, M., Plan, L., 2011. Geomorphology and natural hazards in karst areas: a review. Geomorphology 134, 1–8.
Wang, Y., Luo, Z., Kang, Y., Liu, X., Zuo, H., 2012. Distribution characteristics and prediction of karst collapse induced by dewatering aquifer in mine area. China Saf. Sci. J. 22 (8), 10–14 (In Chinese).
Youssef, A.M., El-Kaliouby, H.M., Zabramawi, Y.A., 2012. Integration of remote sensing and electrical resistivity methods in sinkhole investigation in Saudi Arabia. J. Appl. Geophys. 87, 28–39.
Yuan, D., 2013. Variations of karst geomorphology over geoclimatic gradients. Geomorphology 6, 319–326.
Yilmaz, I., 2007. GIS based susceptibility mapping of karst depression in gypsum: a case study from Sivas basin (Turkey). Eng. Geol. 90, 89–103.
Zhou, G., Chen, K., He, S., Huang, J. and Yan, H., 2014. Data analysis of karst collapse based on GIS: a case study of Jili, Guangxi. In: Proceedings of IEEE Geoscience and Remote Sensing Symposium (IGARSS). Quebec, Canada, pp. 3085–3088.
Zhong, K., Li, Z., Li, M., 1984. Outline of Guangxi Regional geology. Geol. Guangxi 1, 20–30 (In Chinese).
Zhu, S.Z., Zhou, J.H., Chen, X.J., 2000. Analysis of forming conditions and main influential factors of karst collapse in west urban district, Guilin city. J. Guilin Inst. Technol. 20 (2), 100–105 (In Chinese).